ChemComm
Chemical Communications

Accepted Manuscript

This article can be cited before page numbers have been issued, to do this please use: W. Geng and R. Yang, *Chem. Commun.*, 2020, DOI: 10.1039/C9CC09877A.

ROYAL SOCIETY OF CHEMISTRY

rsc.li/chemcomm

View Article Online
DOI: 10.1039/C9CC09877A

Journal Name

COMMUNICATION

Triple-helix molecular switch photoelectrochemical biosensor for ultrasensitive microRNA detection based on position-controllable CdS//CdTe signal enhancing and switching

Received 00th January 20xx,
Accepted 00th January 20xx

DOI: 10.1039/x0xx00000x

www.rsc.org/

Wenchao Geng,[a] and Ruiying Yang*[,a,b]

Herein, a triple-helix molecular switch photoelectrochemical (PEC) biosensor is developed for ultrasensitive and selective detection of microRNA based on position-controllable CdS//CdTe signal enhancing and switching accompanying the signal amplification of three-dimensional DNA walking machine. The developed PEC biosensor exhibits excellent analytical performance for microRNA-141 detection with a wide linear range from 5 aM to 100 fM, a low detection limit of 1.3 aM and outstanding selectivity.

MicroRNAs (miRNAs) as a series of endogenetic, noncoding single-stranded RNAs (ca. 18-25 nt), are crucial regulators in gene transcription, expression, cellular proliferation.[1] Their aberrant expression is closely related to various types of human cancer, and growing evidence has shown that miRNAs serve as a promising biomarker candidates for cancer initiation and progression.[2] However, due to their small size, sequence homology among family members, and ultralow abundance in cells and plasma, ultrasensitive and selective detection of miRNAs is still a severe challenge.[3] Currently, more and more methods have been developed for miRNAs assay, such as surface plasmon resonance,[4] surface-enhanced Raman scattering,[5] fluorescence,[6] electrochemiluminescence,[7] electrochemistry,[8] and photoelectrochemistry.[9] Photoelectrochemical (PEC) biosensor, as a newly emerged and rapidly developing analytical technology in biomarker analysis and early cancer detection, has received currently extensive research interest due to its inherent merits of simple instrumentation, low cost, and easy operation.[10]

Recently, a triple-helix molecular switch based on Hoogsteen and Watson−Crick base pairings as a novel research method is universally applicable and has been studied in DNA sensors due to its independent property of binding sequence.[11] Compared with the traditional double-helix DNA sensors, the triple-helix molecular switch strategy possesses some unique advantages. For example, the triple-helix conformation has better stability than the double-helix DNA and makes more target sequence free, leading to strengthening both the binding affinity and specificity toward the targets, further improving the sensitivity.[12] Nevertheless, only a few works addressed on this triple-helix molecular switch PEC biosensors.[13] For example, Yu et al. reported a signal-off PEC biosensor of HIV-1 based on triple-helix molecular switch.[13*a*] Dai et al. developed a signal-off PEC biosensor via triple-helix molecular switch.[13*b*] However, the signal-off sensors based on triple-helix molecular switch suffer from the capacity of their signal, where only a maximum of 100% signal suppression can be obtained under any experimental conditions.[14] Although the signal-on biosensors can circumvent the disadvantages of the signal-off methods, no matter signal-off and signal-on PEC biosensors suffer from influence of the interferents and background signals. Recently, our research efforts reported a few photocurrent-direction switching PEC sensors, which could avoid the false negative or positive error and showed highly sensitive.[15] For example, a highly selective and sensitive PEC sensor was constructed for thrombin detection based on hemin-induced photocurrent-direction switching of CdS.[15*a*] A sensitive PEC assay of miRNA-155 was developed based on CdSe//NPC-ZnO photocurrent-direction switching system.[15*b*] However, despite this, alternative photocurrent-direction switching system is still relatively scarce. Therefore, according to the advantage of triple-helix molecular switch strategy, rationally designing high-performance PEC biosensors combined novel photocurrent reversal system with triple-helix molecular switch strategy is highly desirable.

Herein, a triple-helix molecular switch PEC biosensor is developed for ultrasensitive and selective detection of miRNA-141 based on position-controllable CdS//CdTe signal enhancing and switching accompanying the signal

[a]*State Key Laboratory of Chemo/Biosensing and Chemometrics, College of Chemistry and Chemical Engineering, Hunan University, Changsha, 410082, P. R. China*
[b]*College of Public Health, Zhengzhou University, Zhengzhou, 450001, China*
E-mail: yangruiying@zzu.edu.cn

Electronic Supplementary Information (ESI) available: Experimental details; electrochemical properties of CdS and CdTe; Position-controllable CdS//CdTe signal enhancing and switching mechanism; optimization of experimental conditions; comparison of various methods for miRNA-141 detection; selectivity, reproducibility and stability; recovery tests; TEM images and UV-Vis absorption spectra of Au NRs and Au@Ag NBs;PAGE analysis. See DOI: 10.1039/x0xx00000x

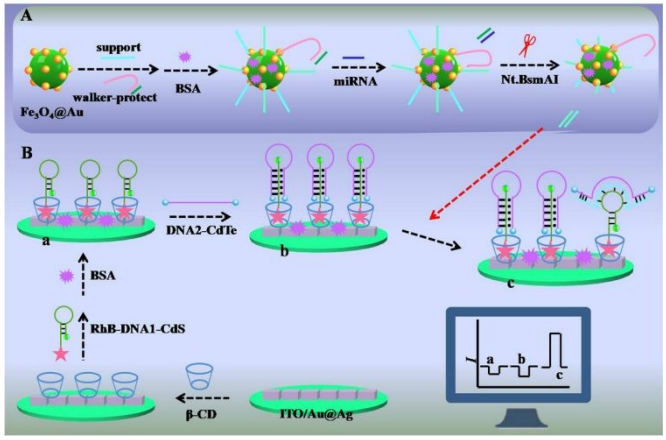

Scheme 1 (A) Process of the 3D DNA walker machine for target amplification, (B) schematic illustration of the developed PEC biosensor based on position-controllable CdS//CdTe signal enhancing and switching.

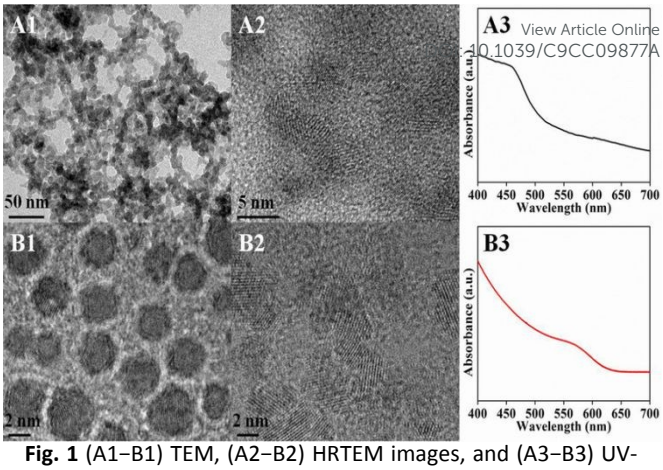

Fig. 1 (A1–B1) TEM, (A2–B2) HRTEM images, and (A3–B3) UV-vis absorption spectra of (A) CdS and (B) CdTe QDs.

amplification of three-dimensional (3D) DNA walking machine. In this PEC system (Scheme 1A), we develop a DNA walker by magnetically responsive Au-coated ferriferrous oxide nanoparticles (Fe_3O_4@Au NPs) as a platform to effectively load and separate DNAs combined with Nt.BsmAI nicking endonuclease to hydrolyze the corresponding recognition sequences, which can convert target miRNAs to numerous transformational DNAs and achieve target amplification. As shown in Scheme 1B, SH-β-cyclodextrin (β-CD) is introduced to the Au@Ag core–shell nanocuboids (NBs)-modified ITO electrode surface via Ag–S bonds. Then, a hairpin RhB-DNA1 modified with CdS QDs (RhB-DNA1-CdS) is introduced to the above electrode through the host-guest interaction between β-CD and RhB. On this PEC biosensing platform, Au@Ag core–shell NBs work as a carrier to anchor β-CD via Ag-S bond and an electron mediator with good conductivity to facilitate electron transfer (Fig. S1, ESI†). RhB is a label of DNA to introduce DNA onto the surface of the modified electrode and is a sensitizing dye to enhance the PEC performance of CdS QDs (Fig. S2, ESI†).[16] Afterward, a single-strand DNA modified with two CdTe quantum dots (CdTe-DNA2) on each end hybridizes with RhB-DNA1-CdS to form a triple-helix conformation, which achieves a cathodic signal enhancing because the CdS is sensitized by CdTe. Subsequently, the relative position between CdS and CdTe is adjusted with the help of the above transformational DNAs, leading to the high-efficiency photocurrent-direction switch from cathodic to anodic photocurrents due to the effective transfer of photo-generated electrons to the ITO electrode with the simultaneous transfer of electrons from CdTe to CdS through the well-matched energy levels. Such a position-controllable PEC enhancing and switching strategy accompanying the triple-helix molecular switch and signal amplification of 3D DNA walker not only affords a ultrasensitivity (1.3 aM) and wide range (5 aM to 100 fM) for miRNA detection, but also avoids the false positive or negative signal and the background signal, which may provide promising applications in early detection of cancers.

The morphology and microstructure of CdS and CdTe QDs were characterized by transmission electron microscopy (TEM) and high-resolution TEM (HRTEM) images shown in Fig. 1. As shown, these nanoparticles appear as pherical particles with the sizes corresponding to about 8 nm and 5 nm, respectively. Such uniform morphologies imply their suitability for the construction of homogeneous photo-responsive films and production of stable PEC signals.[18] Moreover, the HRTEM images (Fig. 1A2–B2) also indicate that these nanoparticles have relatively good crystallinity. Besides, from the UV–vis absorption spectra of CdS and CdTe QDs (Fig. 1A3–B3), broad absorption ranges can be observed, indicating that these nanoparticles have good absorption properties to visible light. Also, to observe the electrochemical properties of CdS and CdTe, the conduction band (CB) and the valence band (VB) of CdS and CdTe are investigated by electrochemical method (Fig. S3, ESI†), which will be useful for understanding the PEC behaviors of the designed CdS//CdTe system.

To further evaluate the feasibility of the proposed strategy, the interaction effect between CdS and CdTe on photocurrent response was investigated (Fig. 2). From Fig. 2A, it is noted that the ITO/CdTe electrode generates a very small cathodic photocurrent (curve a, -82.56×10^{-3} μA). And a big cathodic photocurrent is obtained for the ITO/CdS electrode (-3.386 μA, curve b). When the concentrations of CdTe are quite low, the cathodic photocurrent of the ITO/CdS/CdTe electrode increases with the increasing of CdTe concentration, which can be explained that the CdS is sensitized by CdTe.[15,18] When the concentration of CdTe is further increased, both cathodic and anodic photocurrents are produced on the electrode (curves e and f). Further increasing of the CdTe concentration results in that only anodic photocurrent can be observed and the anodic photocurrent increases with the increasing of the CdTe concentration (curves g, h and i). This implies that the photo-induced electrons transfer to the ITO electrode with the simultaneous transfer of electrons from CdTe to CdS. From Fig. 2C, with the gradual increasing of the CdS concentration, the enhanced cathodic photocurrents of the ITO/CdTe/CdS electrode is obtained, but the photocurrent direction of the electrode cannot change (curves j-m).

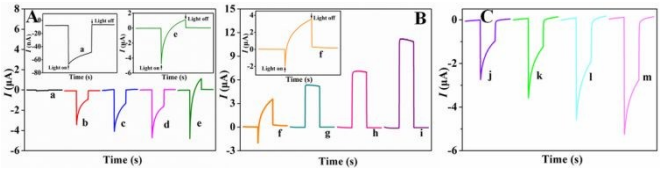

Fig. 2 (A-B) Photocurrent responses of (a) ITO/CdTe electrode, and (b-i) ITO/CdS electrode after incubation with CdTe. The volume of CdTe solution, 20 μL; (b) 0, (c) 1000-fold, (d) 500-fold, (e) 100-fold, (f) 50-fold, (g) 10-fold, (h) 5 and (i) 1-fold (CdTe solution diluted by H_2O, CdTe incubation time, 10 min). (C) (j-m) ITO/CdTe electrode after incubation with CdS. The volume of CdS solution: (j) 5 μL, (k) 20 μL, (l) 50 μL, (m) 100 μL (CdS incubation time, 2 h). The PEC tests are carried out in 0.1 M Tril-HCl (pH 7.4) containing 0.1 M AA under visible light illumination (λ > 420 nm).

As an effective way for characterizing the electrode interface, electrochemical impedance spectroscopy (EIS) was used to reveal the fabrication process of the biosensor. From Fig. 3A, ITO/Au@Ag electrode reveals a very small charge transfer resistance (R_{ct}) value (21.2 Ω, curve a), because of the excellent electrical conductivity of Au@Ag NBs. However, a large R_{ct} value (67.5 Ω, curve a) can be observed after introduction of β-CD on the electrode surface owe to the poor electrical conductivity of β-CD. Subsequently, the self-assembly of RhB-DNA1-CdS increase the R_{ct} value (88.2 Ω, curve c) because the CdS and DNA molecules hinder the electron transfer, indicating that RhB-DNA-CdS is successfully attached to the electrode through the host-guest interaction between β-CD and RhB. Then, blocking of the surface with BSA further results in an enhanced R_{ct} value (107.6 Ω, curve d). The hybridization between DNA2-CdTe and RhB-DNA1-CdS makes the R_{ct} value increase to 130.4 Ω (curve e), suggesting the successful formation of the triple-helix molecular structure. When the modified electrode is incubated with transformational DNAs, the hybridization is occurred in RhB-DNA1-CdS, transformational DNAs and DNA2-CdTe, leading to an increased R_{ct} value (147.5 Ω, curve e). The results suggest that the proposed miRNA PEC biosensor is successfully fabricated (Scheme 1).

To further monitor the stepwise modification of our designed biosensing strategy, PEC response was recorded in Fig. 3B. Comparing with the extremely weak photocurrent of ITO/Au@Ag electrode (curve a), the photocurrent response with the modification of β-CD closing to zero is obtained (curve b), because of the poor charge transmission of β-CD. After the modification of RhB-DNA1-CdS, a large cathodic photocurrent response can be seen (curve c), due to the excellent photoelectric activity of CdS and RhB. Subsequent surface modification with BSA leads to a decreased photocurrent (curve d). When DNA2-CdTe is introduced to the sensing platform via pairing with RhB-DNA-CdS, the cathodic photocurrent significantly enhances (curve e), which is caused by the sensization effect of CdTe, according to the possible photocurrent generation mechanism shown in Scheme S1D (ESI†). However, when transformational DNAs are hybridized with triple-helix molecular conformation between RhB-DNA1-

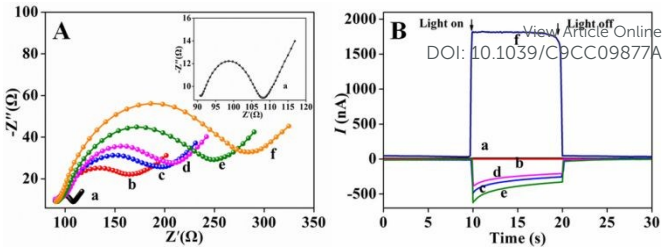

Fig. 3 (A) EIS results and (B) Photocurrent responses of different electrodes: (a) ITO/Au@Ag, (b) ITO/Au@Ag/HS-β-CD, (c) ITO/Au@Ag/HS-β-CD/RhB-DNA1-CdS, (d) ITO/Au@Ag/HS-β-CD/RhB-DNA1-CdS/BSA, (e) ITO/Au@Ag/HS-β-CD/RhB-DNA1-CdS/BSA/DNA2-CdTe, (f) ITO/Au@Ag/HS-β-CD/RhB-DNA1-CdS/BSA/DNA2-CdTe/transformational DNA corresponding to 5 fM miRNA-141.

CdS and DNA2-CdTe, the high-efficiency photocurrent-direction switching from cathodic photocurrent (-629.15 nA, curve e) to anodic photocurrent (1725.7 nA, curve f) is surveyed. The surprising result should be ascribed as follows: such DNA configuration change adjusts the relative position of CdS and CdTe, and the matched energy levels between CdS and CdTe prompt the photo-generated electrons transfer from the VB of CdTe to the VB of CdS, resulting in an improved separation of e^-/h^+ pairs, according to the CdTe-induced photocurrent-direction switching (Fig. 2) and the possible photocurrent generation mechanism (Scheme S1B, ESI†).

Under optimal experimental condition (Fig. S5A–B, ESI†), our designed PEC biosensing platform was used for miRNA-141 detection. In the presence of miRNA-141, the photocurrent direction of the PEC biosensor is switched from cathode (background signal) to anode (Fig. 4A), which indicates that the proposed biosensor possesses super anti-interference ability to eliminate a false negative or positive error, because the common interferents just cause the enhancement or decrement of the photocurrent and cannot switch the photocurrent direction. Additionally, the anodic photocurrent increases with the increasing miRNA-141 concentration (Fig. 4A). From Fig. 4B, the photocurrent response shows an excellent liner relationship with the logarithm of miRNA-141 concentration from 5 aM to 100 fM, and the linear regression equation is I = 298.7 + 384.0 lg$C$ (R^2 = 0.9975) with a detection limit of 1.3 aM (3σ). As shown in Table S2 (ESI†), the proposed

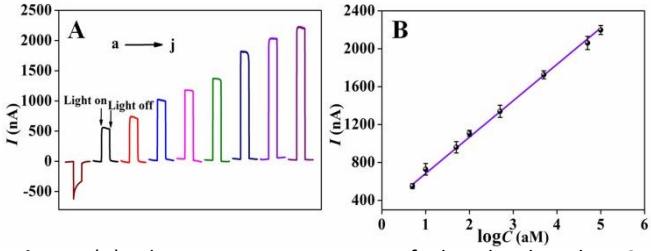

Fig. 4 (A) Photocurrent responses of the developed PEC biosensor to miRNA-141 from (a) to (i): 0, 5, 10, 50, 100, 500, 5000, 50000, and 100000 aM. (B) Corresponding calibration plot between the logarithm of the miRNA-141 concentration and I value.

PEC assay shows an outstanding improvement in analytical performance compared with most of other biosensing systems, which is ascribed to the fantastic introduction of triple-helix molecular conformation, 3D DNA walker machine signal amplification and position-controllable CdS//CdTe signal enhancing and switching strategy. On the other hand, the developed PEC biosensing platform shows outstanding selectivity, good reproducibility, acceptable stability, and satisfactory recovery in complex biological system (ESI†).

In summary, based on 3D DNA walking machine induced signal amplification and triple-helix molecular switch position-based electron transfer induced signal enhancing and switching strategy, a novel PEC biosensor is developed for ultrasensitive and selective detection of microRNA. Main characteristics and advantages are as follows: (1) the 3D DNA walking machine with high-efficiency payload releasing and excellent signal amplification is introduced in the PEC biosensing platform for converting target microRNA to transformational DNA; (2) the triple-helix molecular switch arranges meaningly the relative position between CdS and CdTe to improve enhancing effect of the background signal; (3) the cleverly designed high-efficiency photocurrent-direction switching strategy depending on position-based electron transfer between CdS and CdTe not only avoids the false positive or negative signal and the background signal but also affords an ultrasensitivity. Considering these advantages, the proposed PEC biosensor exhibits a linear range from 5 aM to 100 fM and a low detection limit of 1.3 aM for microRNA-141 detection, which may have promising applications in biomedical and clinical diagnosis.

Conflicts of interest

There are no conflicts to declare.

Notes and references

1 (*a*) Z. H. Xu, H. Wang, J. Wang, W. W. Zhao, J. J. Xu and H. Y. Chen, *Anal. Chem.* 2019, **91**, 12000–12005; (*b*) X. H. Pang, X. Zhang, K. K. Gao, S. Wan, C. Cui, L. Li, H. B. Si, B. Tang and W. H. Tan, *ACS Nano* 2019, **13**, 1817–1827.

2 (*a*) X. Huang, Y. Liu, B. Yung, Y. Xiong and X. Chen, *ACS Nano* 2017, **11**, 5238−5292; (*b*) C. Ye, M. Q. Wang, Z. F. Gao, Y. Zhang, J. L. Lei, H. Q. Luo and N. B. Li, *Anal. Chem.* 2016, **88**, 11444−11449.

3 (*a*) T. Hou, W. Li, X. J. Liu and F. Li, *Anal. Chem.* 2015, **87**, 11368−11374; (*b*) W. H. Dai, H. F. Dong, B. Fugetsu, Y. Cao, H. T. Lu, X. L. Ma and X. J. Zhang, *Small* 2015, **11**, 4158–4164.

4 X. M. Li, W. Cheng, D. D. Li, J. L. Wu, X. J. Ding, Q. Cheng and S. J. Ding, *Biosens. Bioelectron.* 2016, **80**, 98−104.

5 (*a*) J. Su, D. F. Wang, L. Nörbel, J. L. Shen, Z. H. Zhao, Y. Z. Dou, T. H. Peng, J. Y. Shi, S. Mathur, C. H. Fan and S. P. Song, *Anal. Chem.* 2017, **89**, 2531–2538; (*b*) Y. C. Song, T. L. Xu, L. P. Xu and X. J. Zhang, *Nanoscale,* 2018, **10**, 20990–20994.

6 (*a*) B. C. Yin, Y. Q. Liu and B. C. Ye, *J. Am. Chem. Soc.* 2012, **134**, 5064–5067; (*b*) C. L. Li, H. K. Li, J. J. Ge and G. F. Jie, *Chem. Commun.* 2019, **55**, 3919–3922.

7 (*a*) M. J. Li, C. Xiong, Y. N. Zheng, W. B. Liang, R. Yuan and Y. Q. Chai, *Anal. Chem.* 2018, **90**, 8211−8216; (*b*) J. Lu, L. Wu, Y. F. Hu, S. Wang and Z. Y. Guo, *Biosens. Bioelectron.* 2018, **109**, 13–19; (*c*) Y. Z. Wang, S. Y. Ji, H. Y. Xu, W. W. Zhao, J. J. Xu and H. Y. Chen, *Anal. Chem.* 2018, **90**, 3570–3575.

8 (*a*) H. V. Tran, B. Piro, S. Reisberg, H. T. Duc and M.C. Pham, *Anal. Chem.* 2013, **85**, 8469−8474; (*b*) T. L. Xu, Y. C. Song, W. Gao, T. T. Wu, L. P. Xu, X. J. Zhang and S. T. Wang, *ACS Sens.* 2018, **3**, 72−78.

9 (*a*) C. Ye, M. Q. Wang, H. Q. Luo and N. B. Li, *Anal. Chem.* 2017, **89**, 11697−11702; (*b*) N. Zhang, X. M. Shi, H. Q. Guo, X. Z. Zhao, W. W. Zhao, J. J. Xu and H. Y. Chen, *Anal. Chem.* 2018, **90**, 11892–11898; (*c*) Y. N. Zheng, W. B. Liang, C. Y. Xiong, Y. Zhuo, Y. Q. Chai and R. Yuan, *Anal. Chem.* 2017, **89**, 9445−9451.

10 (*a*) Y. Gu, J. Song, M. X. Li, T. T. Zhang, W. Zhao, J. J. Xu, M. L. Liu, H. Y. Chen, *Anal. Chem.* 2017, **89**, 10585–10591; (*b*) R. Y. Yang, K. Zou, Y. M. Li, L. X. Meng, X. H. Zhang and J. H. Chen, *Anal. Chem.* 2018, **90**, 9480–9486; (*c*) Z. B. Luo, L. J. Zhang, R. J. Zeng, L.S. Su and D. P. Tang, *Anal. Chem.* 2018, **90**, 9568–9575; (*d*) R. Y. Yang, X. X. Yan, Y. M. Li, X. H. Zhang and J. H. Chen, *ACS Appl. Mater. Interfaces* 2017, **9**, 42482−42491; (*e*) R. Y. Yang, Y. M. Li, K. Zou, L. X. Meng, X. H. Zhang and J. H. Chen, *Chem. Commun.* 2018, **54**, 4830–4833; (*f*) J. F. Chang, X. Wang, J. Wang, H. Y. Li and F. Li, *Anal. Chem.* 2019, **91**, 3604−3610.

11 (*a*) T. N. Grossmann, L. Röglin and O. Seitz, *Angew. Chem., Int. Ed.* **2007**, *46*, 5223−5225; (*b*) X. Z. Wang, A. W. Jiang, T. Hou and F. Li, *Analyst* 2014, **139**, 6272−6278.

12 (*a*) H. Gao, J. F. Zhang, Y. Liu, W. W. Tu, T. X. Wei and Z. H. Dai, Anal. Chem.2019, **91**, 12038–12045; (*b*) Z. Zou, H. Yang, Q. Yan, P. Qi, Z. H. Qing, J. Zheng, X. Xu, L. H. Zhang, F. Feng and R. H. Yang, *Chem. Commun.* 2019, **55**, 6433–6436.

13 (*a*) S. P. Wang, J. G. Zhao, Y. Zhang, M. Yan, L. N. Zhang, S. G. Ge and J. H. Yu, *Biosens. Bioelectron.* 2019, **139**, 111325; (*b*) Y. Zang, J. P. Lei, L. Zhang and H. X. Ju, *Anal. Chem.* 2014, **86**, 12362–12368.

14 (*a*) Z. G. Yu and R. Y. Lai, *Chem. Commun.* 2012, **48**, 10523−10525; (*b*) L. Wu, X. H. Zhang, W. Liu, E. H. Xiong and J. H. Chen, *Anal. Chem.* 2013, **85**, 8397−8402.

15 (*a*) R. Y. Yang, K. Zou, X. H. Zhang, C. C. Du and J. H. Chen, *Chem. Commun.* 2019, **55**, 8939–8942; (*b*) L. X. Meng, Y. M. Li, R. Y. Yang, X. H. Zhang, C. C. Du and J. H. Chen, *Chem. Commun.* 2019, **55**, 2182–2185.

16 (*a*) X. X. Yan, J. J. Li, R. Y. Yang, Y. M. Li, X. H. Zhang and J. H. Chen, *Sens. Actuators, B*, 2018, **255**, 2187–2193; (*b*) T. Iwamoto, Y. Ogawa, L. Sun, M. S. White, E. D. Glowacki, M. C. Scharber, N. S. Sariciftci, K. Manseki, T. Sugiura, and T. Yoshida, *J. Phys. Chem. C* 2014, **118**, 16581–16590.

17 Q. Wang, Y. F. Ruan, W. W. Zhao, P. Lin, J. J. Xu and H. Y. Chen, *Anal. Chem.* 2018, **90**, 3759–3765.

18 (a) M. J. Li, Y. N. Zheng, W. B. Liang, Y. L. Yuan, Y. Q. Chai and R. Yuan, *Chem. Commun.* 2016, **52**, 8138–8141; (*b*) H. H. Wang, M. J. Li, Y. N. Zheng, T. Hu, Y. Q. Chai and R. Yuan, *Biosens. Bioelectron.* 2018, **120**, 71−76; (*c*) H. H. Wang, M. J. Li, H. J. Wang, Y. Q. Chai and R. Yuan, *ACS Appl. Mater. Interfaces* 2019, **11**, 23765–23772.